# The Possible Photochemical Origins of Banded Iron Formations

by

Parker Castleberry

A Thesis Presented in Partial Fulfillment
of the Requirements for the Degree
Master of Science

Approved June 2017 by the
Graduate Supervisory Committee:

Ariel Anbar, Chair
Pierre Herckes
James Lyons

ARIZONA STATE UNIVERSITY

August 2017

# ABSTRACT

Banded iron formations (BIFs) are among the earliest possible indicators for oxidation of the Archean biosphere. However, the origin of BIFs remains debated. Proposed formation mechanisms include oxidation of Fe(II) by $O_2$ (Cloud, 1973), photoferrotrophy (Konhauser et al., 2002), and abiotic UV photooxidation (Braterman et al., 1983; Konhauser et al., 2007). Resolving this debate could help determine whether BIFs are really indicators of $O_2$, biological activity, or neither.

To examine the viability of abiotic UV photooxidation of Fe, laboratory experiments were conducted in which Fe-bearing solutions were irradiated with different regions of the ultraviolet (UV) spectrum and Fe oxidation and precipitation were measured. The goal was to revisit previous experiments that obtained conflicting results, and extend these experiments by using a realistic bicarbonate buffered solution and a xenon (Xe) lamp to better match the solar spectrum and light intensity.

In experiments reexamining previous work, Fe photooxidation and precipitation was observed. Using a series of wavelength cut-off filters, the reaction was determined not to be caused by light > 345 nm. Experiments using a bicarbonate buffered solution, simulating natural waters, and using unbuffered solutions, as in prior work showed the same wavelength sensitivity. In an experiment with a Xe lamp and realistic concentrations of Archean [Fe(II)], Fe precipitation was observed in hours, demonstrating the ability for photooxidation to occur significantly in a simulated natural setting.

These results lead to modeled Fe photooxidation rates of 25 mg Fe $cm^{-2}$ $yr^{-1}$—near the low end of published BIF deposition rates, which range from 9 mg Fe $cm^{-2}$ $yr^{-1}$

to as high as 254 mg Fe $cm^{-2}$ $yr^{-1}$ (Konhauser et al., 2002; Trendall and Blockley, 1970). Because the rates are on the edge and the model has unquantified, favorable assumptions, these results suggest that photooxidation could contribute to, but might not be completely responsible for, large rapidly deposited BIFs such those in the Hamersley Basin. Further work is needed to improve the model and test photooxidation with other solution components. Though possibly unable to fully explain BIFs, UV light has significant oxidizing power, so the importance of photooxidation in the Archean as an environmental process and its impact on paleoredox proxies need to be determined.

# ACKNOWLEDGMENTS

I would like to acknowledge the incredible support of my advisor, Ariel Anbar. Steve Romaniello also provided me with indispensable guidance and tactical support. Thank you to everyone in the Anbarlab group for their help. I cannot thank my parents enough for the counsel they provided. I am grateful to my committee members Dr. Herckes and Dr. Lyons for their input. I must thank Dr. Pepper for sustaining me every morning.

Most importantly, this includes but is not limited to all the above, I could not have done this without the encouragement of those who believed in me.

TABLE OF CONTENTS

Page

CHAPTER Page

LIST OF TABLES

Table Page

LIST OF FIGURES

Figure Page

CHAPTER 1 INTRODUCTION

Starting about two and a half billion years ago Earth underwent a dramatic change in its geological, chemical and biological environment as the atmosphere quickly accumulated $O_2$. In about 100 million years, atmospheric $O_2$ levels increased over than 1 ppm ($10^{-5}$ times the present atmospheric level (PAL)) on its way to modern levels (Fig. 1) (Lyons et al., 2014).

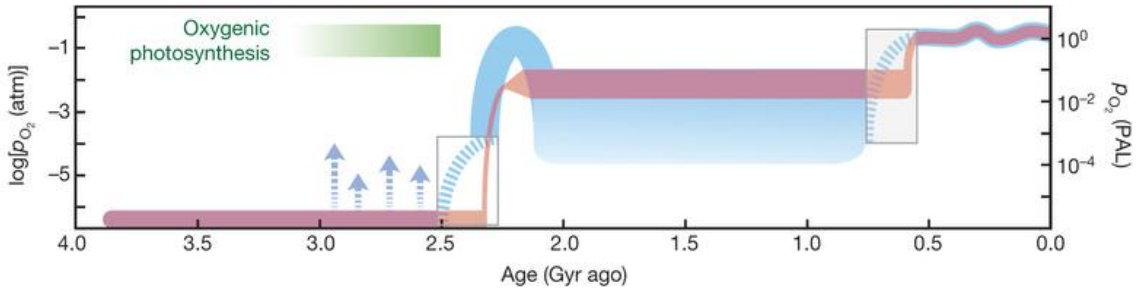


Figure 1. Atmospheric $O_2$ levels over time. The Great Oxygenation Event (GOE) occurred between 2.4 and 2.3 billion years ago (Gyr ago) (Luo et al., 2016). The orange denotes the classical view of Earth's oxygen history while the blue indicates newer theories. Figure from Lyons et al. (2014).

As $O_2$ is largely produced by oxygenic photosynthetic organisms (cyanobacteria) (Holland and Schidlowski, 1982), past $O_2$ levels can inform us of not only geochemical conditions but also early biological activity as well. Understanding the GOE is linked to understanding the evolution of the Earth's early biosphere. Though the GOE was such a fundamental shift, details such as the timing and tempo remain unclear (Lyons et al., 2014). For example, there is evidence that transient amounts of $O_2$ appeared as much as 500 million years before signs of pervasive global atmospheric $O_2$ > 1 ppm (Anbar et al., 2007; Farquhar et al., 2000; Planavsky et al., 2014).

One of the first identified indicators of past $O_2$ are banded iron formations (BIFs) (Cloud, 1973). These sedimentary ferric iron oxide deposits can be hundreds of meters thick, over 100,000 $km^2$ in area, and contain trillions of tons of Fe (Bekker et al., 2010). They were originally interpreted to be formed by biologically produced $O_2$ that oxidized dissolved Fe(II) in the oceans (Cloud, 1973; Holland, 1973), leading to precipitation of Fe(III) oxyhydroxides. However, this model was contested as early as the late 1970's (Cairns-Smith, 1978). Two alternative mechanisms not involving $O_2$ have been proposed. One mechanism is the direct metabolic oxidation of Fe(II) by microorganisms using anoxygenic photosynthesis—a process called photoferrotrophy (Konhauser et al., 2002). The second proposed mechanism is that Fe(II) was directly oxidized by ultraviolet (UV) light (Cairns-Smith, 1978). This photooxidation mechanism would not require biological activity at all. Today, photoferrotrophy is the widely accepted $O_2$ alternative, while the literature exploring photooxidation has contradictions and lacks testing in realistic conditions. It is therefore unclear if BIFs are signs of $O_2$, life, or neither. Can BIFs be created simply by sunlight and not by biological activity?

The photooxidation mechanism uses ultraviolet light from the sun to directly oxidize aqueous dissolved Fe(II) (e.g. equation 1; Fe(II) complexes other than $Fe(H_2O)_6^{2+}$ may also play a role) (Cairns-Smith, 1978)

$$Fe(H_2O)_6^{2+} + 3\ H_2O + h\nu \rightarrow Fe(OH)_3 + 2\ H^+ + \tfrac{1}{2}H_2 \quad (1)$$

In this scenario, a UV photon would be absorbed by Fe(II) causing an electron to come off, making Fe(III). The mechanism would proceed with hydrolysis by the Fe(III) , creating insoluble $Fe(OH)_3$ or other (oxy)hydroxides (Braterman et al., 1983; Cairns-Smith, 1978). This photooxidation process would take place in the zone of UV light

penetration—from less than one meter to tens of meters depending on wavelength and ocean conditions (Tedetti and Sempéré, 2006). This mechanism was first proposed purely hypothetically in 1978 by Cairns-Smith (Cairns-Smith, 1978).

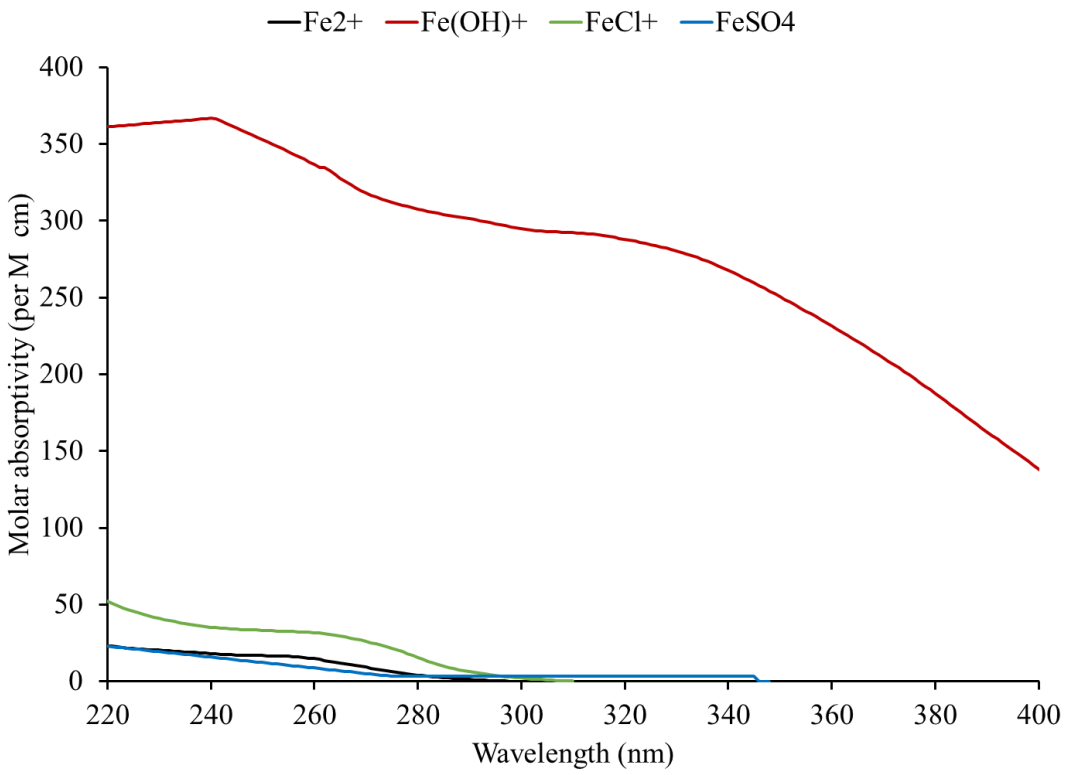


Figure 2. UV molar absorptivity of some Fe(II) species ($Fe(OH)^+$: Ehrenfreund and Leibenguth, 1970; $FeCl^+$: Heinrich and Seward, 1990; $Fe^{2+}$ Potterill et al., 1936; $Fe(SO_4)$: Rigg and Weiss, 1952). $Fe(OH)^+$ has strong absorbance (per unit concentration) relative to other Fe(II) species and absorbs at long wavelengths. $Fe(H_2O)_6^{2+}$ and $FeCl^+$ absorb < 300 nm. $Fe(SO_4)$ absorbs weakly < 350 nm and more strongly < 280 nm.

Several studies attempted to experimentally test the hypothesis but disagree on the wavelengths that cause the photooxidation reaction and therefore come to disparate

conclusions. Braterman et al. (1983) found light longward of 400 nm (i.e. visible) to be effective. Including shorter-wavelength light, down to 200 nm, increased the rate of the reaction. These observations, combined with a photooxidation model, led them to conclude that photooxidation could account for all BIF deposition. Using a more sophisticated model accounting for factors like Fe self-shielding, François (1986) calculated the rate of Fe deposition from photochemistry in the Archean ocean to be 100 – 200 mg Fe $cm^{-2}$ $yr^{-1}$. This value is much greater than geological estimates of Fe accumulation rates in BIFs, which range from 9 – 43 mg Fe $cm^{-2}$ $yr^{-1}$ to as high as 254 mg Fe $cm^{-2}$ $yr^{-1}$ (Konhauser et al., 2002; Trendall and Blockley, 1970) for the Hamersley Basin BIF. Anbar and Holland (1992) noted that BIFs are generally Mn-poor so they explored the relative rates of Fe and Mn photooxidation and constructed an Fe photooxidation model. Mn oxides precipitated very slowly during Fe photooxidation, leading them to conclude photochemistry could account for BIFs in their models (Anbar and Holland, 1992). However, later work by Konhauser et al. (2007) found light with wavelengths 320 – 400 nm did not cause photooxidation, while light at 254 nm was effective.

The wavelength-dependence of the photooxidation reaction is critical for many reasons, both environmental and chemical. Environmental factors are the solar spectrum and depth UV light will reach in water. Sunlight (without an ozone layer blocking UV) has 12 times more irradiance 300 – 450 nm than below 300 nm (Lide, 2004). Longer wavelengths penetrate deeper into the ocean increasing the volume of the "UV photic zone" where photooxidation could take place. Short wave UV (~200 nm) can penetrate only a few millimeters in water while 400 nm light can penetrate meters to tens of meters

depending on ocean conditions (Tedetti and Sempéré, 2006). From a pure photochemistry perspective, long and short-wave UV absorbance by Fe takes place by two different species. Absorbance < 300 nm is dominated by $Fe(H_2O)_6^{2+}$ while > 300nm is due to $Fe(OH)^+$ (Ehrenfreund and Leibenguth, 1970). The absorbance and quantum yield of each species varies. If Konhauser et al.'s observation that only UV-C (100 – 280 nm) causes photooxidation is applied to a model based on Francois (1986), the photooxidation rates become much slower—below BIF geological rates and insignificant compared to that of photoferrotrophy (Konhauser et al., 2007).

In this work, we aimed to reconcile prior experiments, then extend these experiments into more realistic conditions. Previous work has used dissimilar techniques to measure Fe. Braterman et al. (1983) largely inferred photooxidation by pH change, and used the thiocyanate assay—specific for Fe(III)—in some experiments. Konhauser et al. (2007) measured photooxidation by the ferrozine assay for Fe(II). We are measuring pH in some experiments, using ferrozine and thiocyanate to measure Fe oxidation, and quantifying total dissolved Fe by ICP-MS.

Our second goal was to conduct experiments in a more realistic simulation of the Archean environment with regards to solution chemistry and light source. Previous experiments did not use buffered solutions, while we chose to buffer our solution with bicarbonate—the major buffer in natural ocean waters—following the procedure of Anbar and Holland (1992). Carbonate would not only buffer the solution pH, but greatly affect the speciation of Fe(II) by creating Fe carbonate species ($FeHCO_3^+$ and $FeCO_3$). Furthermore, the Archean was thought to have significantly higher atmospheric $CO_2$ (Hessler et al., 2004) than today, making the carbonate system even more important. This

experiment also had a realistic [Fe(II)], 0.18 mM, thought to be the upper limit of the Archean oceans (Holland, 1973) as opposed to 4 mM for earlier experiments (Braterman et al., 1983).

Our second major experimental improvement was in the light source. Previous experiments used Hg lamps which do not match the solar spectrum in both intensity and irradiance distribution (Fig. 3). Braterman et al. (1983) and Anbar and Holland (1992) used medium-pressure Hg lamps that have significant peaks at certain wavelengths such as 366nm. Konhauser et al. scaled their light flux to solar values, but used a low-pressure Hg lamp—with a single sharp peak at 254 nm—and a UV blacklight emitting UV 320 – 400 nm. Their set-up had no light between about 256 and 320 nm. In contrast, Xe lamps emit across a continuous spectrum from 200 to 2700 nm (limited by the absorbance of the fused silica optics), providing a good analogue to the sun (Matson et al., 1984) (Fig. 3). So, in some experiments, we used a Xe lamp to test photooxidation using a realistic light source. In addition, a special filter developed to adjust the Xe spectrum to closer match the sun (in our case a filter for extraterrestrial spectrum with no ozone absorbance) was used. However, we found it creates a better match for only certain wavelengths and a poorer match in others, particularly 295 – 350 nm (Fig. 3).

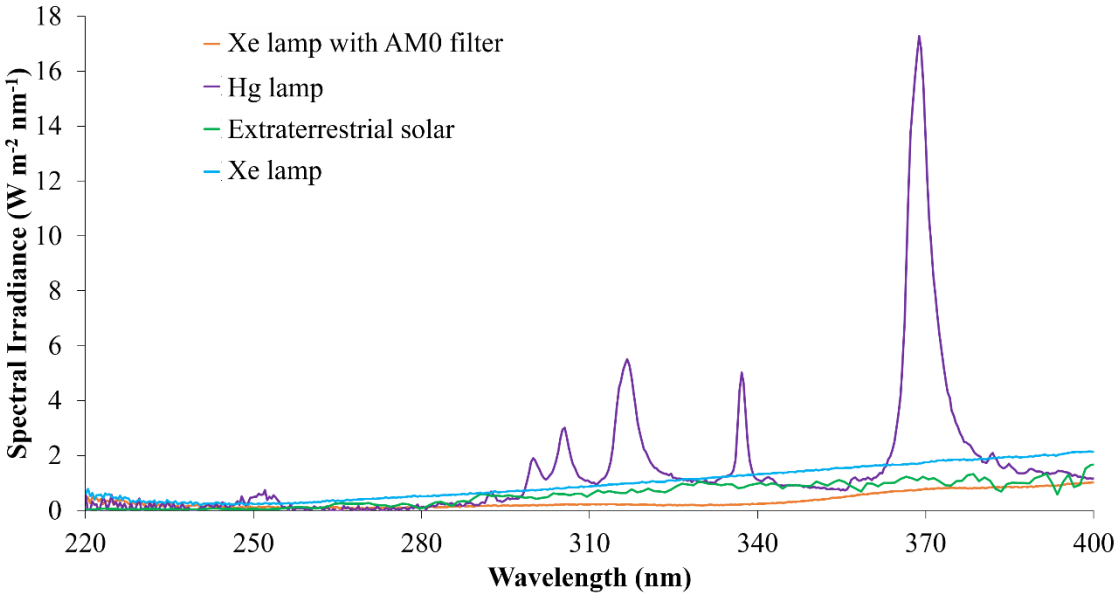


Figure 3. Light source spectra compared to the extraterrestrial (top of the atmosphere) solar spectrum (Gueymard et al., 2002). Note how the Xe lamp has a continuous spectrum without large peaks, while the Hg lamp has very intense spikes.

# CHAPTER 2 MATERIALS AND METHODS

## 2.1 Experiments

The general approach was to conduct laboratory simulations in which deoxygenated Fe(II)-bearing aqueous solutions maintained under an anoxic atmosphere were irradiated with UV-Vis light. To evaluate wavelength dependence we used a series of light filters to block out certain wavelengths. Rates of Fe oxidation were measured over time using the ferrozine assay and thiocyanate assay while precipitation was measured by quadrupole inductively coupled plasma-mass spectrometry (ICP-MS).

### 2.1.1 Experimental setup

To create an anoxic environment, we used a custom-built reaction vessel made of Suprasil UV-transparent quartz, with ports for a pH probe, in-flowing gas, and sampling (Fig. 4). This reactor design was chosen as it is made entirely of quartz and avoids extensive use of plastics, which might allow $O_2$ to diffuse inside over the course of an experiment. Having only 3 small ports minimizes the area of openings.

Solutions consisted of $FeCl_2$ (99.5%, Alfa Aesar), NaCl (99.9% High Purity Grade, Amresco), and in bicarbonate buffered experiments $NaHCO_3$ (99.7% ACS grade, JT Baker) (see below for exact solution compositions) dissolved in Millipore 18.2 MΩ DI $H_2O$.

The solutions were bubbled with 500 mL/min of gas (either Ar or 95% $N_2$/2% $CO_2$ depending on the experiment, see below) over the course of each experiment to ensure the reactor remained $O_2$-free. Alicat Scientific gas flow controllers were used to

maintain a constant gas flow rate and accurately mix the $N_2$ and $CO_2$. Ar or $N_2$ gas was supplied by a dewar (99.998% purity), while the $CO_2$ was from a cylinder (99.5%). Control experiments (Fe with no light) were performed with and without a hot copper $O_2$ scrubber, but it was found to make no difference. To avoid $O_2$ diffusion through plastics in the gas system, stainless steel was used, except for the last ½ meter entering the reactor, where we used PEEK-polymer coated glass capillary tube. Gas was bubbled through a tightly sealed aluminum cylinder of water to humidify the gas and minimize evaporation during the experiment. Aluminum was used because glass would not hold the pressure of the gas system and plastics can diffuse $O_2$ in. The gas system was checked for leaks by filling with He and using He leak detector.

This gas flow bubbling through the reactor solution also served to mix it. We avoided using a stir bar because Teflon stir bars can outgas $O_2$ and glass stir bars can (and did in an early preliminary experiment) crack, releasing air trapped inside.

In all experiments, the light source (either an Hg or Xe lamp) was contained in a Newport lamp housing (Model 66902) with rear reflector and fused silica condenser optics, with 6 cm between the optics and the reactor. To test the wavelength dependence we used a series of wavelength cut-off filters ($\lambda > 400$ nm, $> 345$ nm, and $> 295$ nm). Filters were High Performance Colored Glass Alternative filters from Newport Inc. We tried the Xe lamp with and without a filter to supposedly further correct it to the solar spectrum. This filter for the extraterrestrial solar spectrum is called an Air Mass 0 (AM0) filter (Newport Inc.), as the sunlight is passing though zero atmosphere.

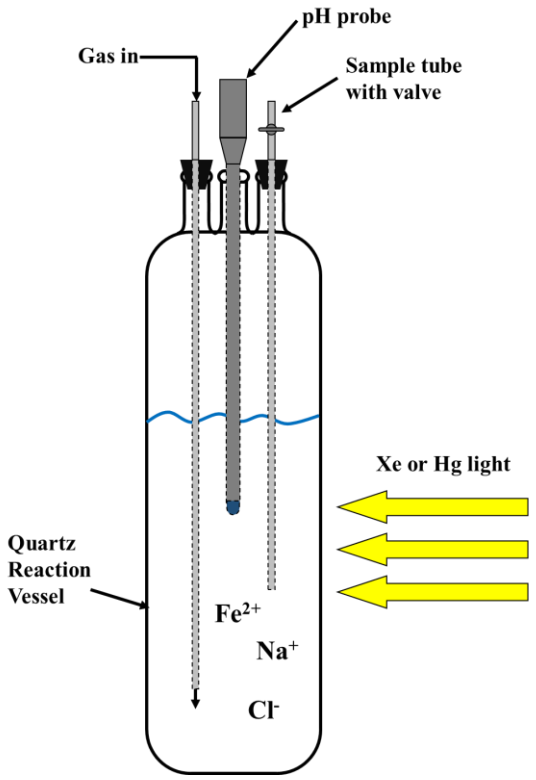


Figure 4. Experimental design. Light from either a Hg or Xe lamp was shined through the side of a quartz vessel containing Fe solutions. The 3 ports at the top were used for the pH probe and venting gas, flowing gas in, and drawing samples.

### 2.1.2 Procedures

Water was deoxygenated by storing in an anaerobic hood for several weeks (pO2 maintained at < 15 ppm), then transferred via flask with rubber stopper to the reactor. The water bubbled in the reaction vessel with the gas (either Ar or 95% $N_2$/2% $CO_2$) for 2 hours prior to the addition of the reagents.

Each experiment was run continuously over a period of 8 to 10 days, periodically swapping out the filters to allow transmission of increasingly shorter wavelengths (i.e. starting with > 400 nm, then > 345 nm, > 295 nm, and no filter). Every experiment began

with a period of dark control (no light) and ended with a second period of no light to ensure any observed oxidation/precipitation was due to the light and that no significant $O_2$ leaked in over the course of the experiment. For these dark periods the reactor was wrapped in Al foil. Each period of dark control, filter, or full spectrum lasted 1 to 2 days.

To quantify the rate of Fe oxidation and precipitation, 2 mL samples were drawn every 12 hours though a disposable 0.2 μm filter into polypropylene syringes. To clear potentially unreacted solution remaining in the sample tube, 3 mL were drawn through the sample tube before taking each sample. A 1 mL aliquot was acidified immediately in 9 mL trace-metal grade 2% $HNO_3$ contained in a Metal-Free (total metals < 1 ppb) polypropylene centrifuge tube (VWR) for later ICP-MS analysis. Aliquots of the remaining solution were measured immediately with ferrozine and thiocyanate assays.

Three types of experiments were conducted. The first type was aimed at reevaluating previous work. To compare to Braterman et al. 1983 and Anbar and Holland 1992, these experiments used a Hg lamp (USHIO 500 W super-high-pressure Hg lamp from Newport, Inc.). The solution composition was nearly identical to that used in Braterman et al. 1983 – 4 mM Fe(II), 0.56 M NaCl in deoxygenated 0.1 mM $H_2SO_4$, adjusted to pH ~7.4 using 0.1 M NaOH. Concentrated $H_2SO_4$ was added to the water, followed by NaCl. After the NaCl dissolved, the pH was adjusted. The solution was bubbled for 2 hours to remove any $O_2$ in the NaOH solution used to adjust pH, then Fe was added. A control experiment was also performed, following the same procedure but with no added Fe. This experiment also used HPLC-grade water to eliminate the possibility of organic compounds reacting.

The second type of experiment was designed to evaluate the relative effectiveness of different wavelength ranges of light to induce Fe photooxidation in a solution of more realistic composition. The solution contained $FeCl_2$ (0.18 mM), NaCl (0.56 M), and $NaHCO_3$ (0.01 M), at pH ~7.3. NaCl and $NaHCO_3$ were added first and allowed to dissolve before the Fe was added. Gas in the experiment was 98% $N_2$ and 2% $CO_2$ – 2% $CO_2$ was chosen as it is not an unreasonable estimate of Archean $pCO_2$ (Hessler et al., 2004). This experiment also used the Hg lamp because it has a higher overall UV flux than the Xe lamp, maximizing the possibility for us detecting a photooxidation reaction if it does occur.

The goal of the third type of experiment tested the capacity for photooxidation with a Xe map to better simulate the solar spectrum. This experiment used the same kind of bicarbonate buffered solution as in the second type of experiments, gas with $CO_2$, as well as the Xe lamp (300 W, Newport Inc.) to approximate the sun.

Table 1. Summary of experiments, goals, and conditions

| Goal | Light source | Gas | Solution composition | Total Duration (days) |
|---|---|---|---|---|
| Reexamine prior experiments especially regarding wavelength dependence | Hg lamp | Ar | Deoxygenated DI water, 4 mM Fe(II), 0.56 M NaCl, 0.1 mM $H_2SO_4$ adjusted to pH ~7.4 using 0.1 M NaOH | 8 |
| Test wavelength dependence using a more realistic solution | Hg lamp | 98% $N_2$/ 2% $CO_2$ | Deoxygenated DI water, 0.18 mM Fe(II), 0.56 M NaCl, 0.01 M $NaHCO_3$, pH ~7.3 | 10 |
| Evaluate the capacity for Fe photooxidation using a realistic solution and light source | Xe lamp | 98% $N_2$/ 2% $CO_2$ | Deoxygenated DI water, 0.18 mM Fe(II), 0.56 M NaCl, 0.01 M $NaHCO_3$, pH ~7.3 | 8 |

After each experiment, the reactor was washed with water, saturated sodium dithionite ($Na_2S_2O_4$) solution to chemically reduce and remove Fe oxides, and 1 M HCl, following the procedure described in Braterman et al. 1983.

Precipitates were recovered by sealing the reactor, transferring it into an anaerobic hood, then emptying the contents of the solution into 50 mL VWR Metal-Free

polypropylene centrifuge tubes. The tubes were centrifuged at about 2000 g for 30 min in a swing-bucket centrifuge, then transferred back into the anaerobic hood where the supernatant was pipetted out. The remaining solution was dried down inside the anaerobic hood before Raman analysis. We dried down the sample instead of filtering it to recover as much Fe precipitate as possible. This method of drying down the sample also caused halite (NaCl) crystals to form from the solution, but this did not pose a problem as halite has no Raman peaks within the scanned range (Downs, 2006).

### 2.1.3 Analytical Methods

Liquid samples were analyzed for total Fe and Na by ICP-MS using a Thermo Scientific iCAP Q. Fe oxidation was evaluated using the ferrozine assay specific for Fe(II) (the technique used by Konhauser et al. 2007) and thiocyanate (SCN) assay for Fe(III) (used by Braterman et al. 1983). Ferrozine is an organic molecule that complexes with Fe(II) and becomes colored ($\lambda_{max}$ of 562 nm) allowing the sample to be analyzed by spectrophotometry (Stookey, 1970), using a Thermo Scientific Genesys 20 instrument. Three separate cuvettes of each sample were prepared to account for differences in the disposable cuvettes (1 cm, 4.5 mL Polystyrene from VWR) used and volume of reagents added, though variations between sample cuvettes were found to typically be < 5%. Thiocyanate complexes with Fe(III), changes color ($\lambda_{max}$ of 480 nm), and was quantified using the same spectrophotometer and cuvettes (Sandell, 1950). Following Sandell (1950) to enhance the sensitivity of the technique we diluted samples in a 50/50 water/acetone mix instead of pure water. Reagent grade acetone was found to cause noticeable coloration in blanks (indicating trace Fe(III)), so semiconductor-grade acetone was used.

Solid precipitates were analyzed using Raman spectroscopy (custom-built instrument using 6 mW 523 nm laser with quartz standard). Raman spectra were analyzed using the RRUFF project CrystalSluth software (Laetsch and Downs, 2006).

### 2.1.4 Actinometry

Overall actinic flux in the UV was determined using the 2-nitrobenzaldehyde (2-NB) actinometer following the procedure described in (Allen et al., 2000). 2-NB absorbs light < 400 nm, and is converted to 2-nitrosobenzoic acid and lowering the pH of the solution. Solution containing 0.1M 2-NB and 0.03M NaOH in 50/50 $H_2O$ and ethanol was prepared in an amber bottle. For the measurements, 200 mL was added to the reactor with the pH probe in and either the Hg or Xe lamp turned on. The procedure is an acid/base titration, with the acid coming from the photochemical reaction. The pH was recorded every 3 minutes until it reached the end-point of 8.5. Equation 2 was used to calculate the photon flux.

$$n = ((10^{pH_{(init)}} - 10^{pH_{(fin)}}) * 2 * N * V ) / (A * t) \quad (2)$$

n = photon flux (photons/$cm^2$*s)
A = cross section area illuminated ($cm^2$), 11.34 $cm^2$ for our set up
t = irradiation time to endpoint in seconds
N = Avogadro's number
V = volume of solution in L (0.2 L)

### 2.1.5 Spectral Measurements

Lamp spectra were measured with an Ocean Optics Flame fiber optic spectrometer with integrating sphere, calibrated for absolute irradiation measurements from the manufacturer, and collected with OceanView software.

## 2.2 Modeling

### 2.2.1 Thermodynamic Calculations

Thermodynamic calculations for solution speciation were carried out using the computer program PHREEQC Interactive version 3.3.5, developed by the U.S. Geological Survey (Parkhurst and Appelo, 2013).

### 2.2.2 Archean Ocean Model

To extrapolate experimental results to the ocean, a model is necessary to calculate the rate of Fe photooxidation. Our model was based on Francois (1986).

$$R = 0.5 \frac{1}{N^A} \int_0^{+\infty} dz \int_{200\ nm}^{X\ nm} \Phi\ \varepsilon_{Fe(OH)^+}(\lambda)\ [Fe(OH)^+]\ F_\lambda(z) d\lambda \quad (3)$$

R is the Fe photooxidation rate in mol Fe per unit area and unit time (area and time units are determined by the units used for the solar flux)

0.5 accounts for day-night cycle

$N^A$ is Avogadro's Number, $6.022 \times 10^{23}$

z is depth, λ is wavelength

X is the longest wavelength the photooxidation reaction is sensitive to

Φ is the quantum yield

$\varepsilon_{Fe(OH)^+}(\lambda)$ is the molar absorptivity of $Fe(OH)^+$ at wavelength λ

[$Fe(OH)^+$] is the concentration of $Fe(OH)^+$ in the water

$F_\lambda(z)$ is photon flux at depth z and wavelength λ

$$F_\lambda(z) = F_\lambda(0)e^{(-\kappa_\lambda z/\cos\chi)} \quad (4)$$

Fλ(0) is incident solar photon flux at wavelength λ

χ is the angle of light in the water from vertical

κλ is attenuation by water and self-shielding by Fe(OH)+ at wavelength λ

$$\kappa_\lambda = \kappa_{H_2O}(\lambda) + \varepsilon_{Fe(OH)^+}(\lambda)[\mathrm{Fe(OH)^+}] \quad (5)$$

This model accounts for self-shielding by $Fe(OH)^+$ and does not assume a specific depth for the UV photic zone. Instead it uses an indefinite integral with respect to depth, letting the absorbance of water and Fe species attenuate the light, as happens in the natural ocean.

The shortest wavelength is set by atmospheric absorbance. The Archean atmosphere did not have an ozone layer blocking UV < 300 nm (because there was extremely low $O_2$) (Kasting and Donahue, 1980), but $CO_2$ and $H_2O$ vapor in an atmosphere would block light < 200 nm (Ranjan and Sasselov, 2016). The longest wavelength, X, is determined by experiments. Francois (1986) used 460 nm, based on $Fe(OH)^+$ absorbance and Braterman et al.'s (1983) finding of photooxidation > 400 nm. This parameter is adjusted to explore ramifications of different experimental findings.

For $F_\lambda(0)$ we used a solar spectrum calculated for a 2.7 Ga sun (Claire et al., 2012). This spectrum is based on the latest, most sophisticated stellar models and observations of sun-like stars. Using this spectrum is an improvement on the previous

photochemical models, which assumed simple scaling values (the current state of knowledge at the time). Anbar and Holland (1992) used a UV flux < 300 nm that was double modern values while Braterman et al. (1983) and Francois (1986) assumed the sun was uniformly 25-30% fainter (Fig. 5). For $\kappa_W$ we used values for natural seawater taken from Smith and Baker, (1981).

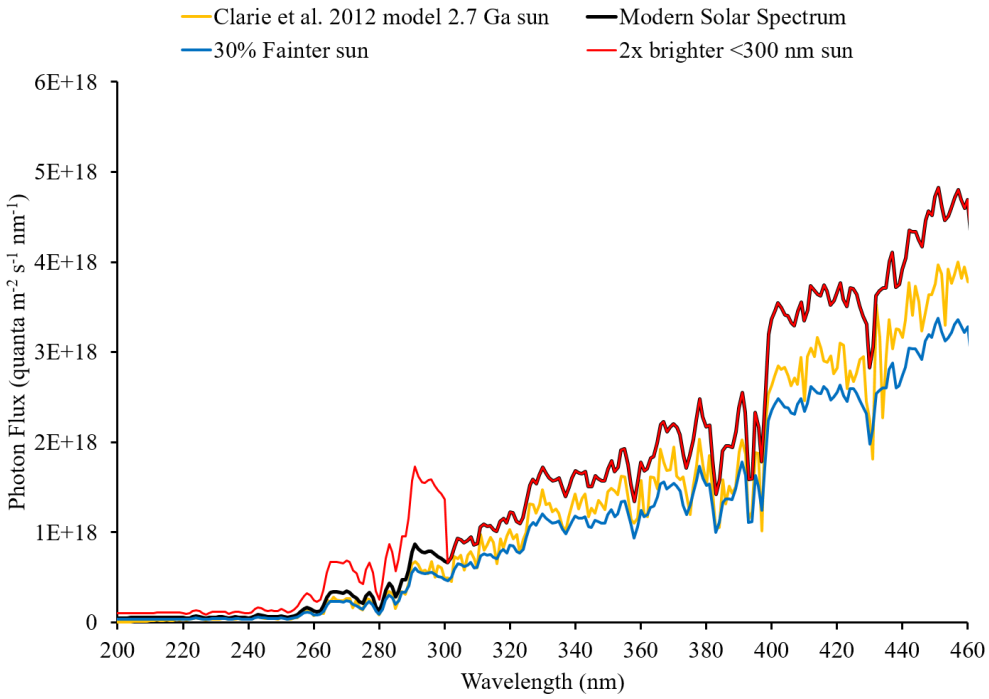


Figure 5. Comparison of the solar spectra used in various models. All are for the extraterrestrial (i.e. with no atmospheric absorbances). The calculated flux a 2.7 Ga sun from Claire et al. (2012) lies between the modern spectrum and the 30% fainter sun used in some previous models, while a sun twice bright < 300 nm is an overestimate over the new models. It is not incorrect to say that the sun was likely brighter in the UV during the Archean, however only for wavelengths < 200 nm (Claire et al., 2012).

# CHAPTER 3 RESULTS

## 3.1 Experiments

### 3.1.1 Replication of Previous Work

During the 48-hour control period with the Hg lamp off, no precipitation of Fe was observed. In fact, concentrations of total dissolved Fe (measured by ICP-MS) increased by about 9%. This increase can be attributed to evaporation over the course of the experiment as measured Na concentrations also increased. To correct for evaporation, [Total Fe] was ratioed to [Na] (Fig. 6). [Total Fe] was used because it was measured using the same method as [Na] (quadrupole ICP-MS). The [Fe]/[Na] ratio reveals no trend (a linear regression has a slope of $-1.46 \times 10^{-4} \pm 1.83 \times 10^{-4}$) demonstrating that increases in [Total Fe] from evaporation did not mask any subtle decreases from precipitation.

When the Hg lamp was switched on with a filter for wavelengths > 400 nm in place, no decrease in [Fe]/[Na] was observed over 48 hours (Fig. 6). The pH however, did respond to the light, decreasing by about 0.2 units in 2 hours.

The filter for wavelengths > 345 nm also showed no precipitation in 48 hours, but the pH again did go down slightly (about 0.1 units in 2 hours) (Fig. 6). There was a slow pH drift of about 1 unit downward over 5 days. Thiocyanate measurements did not detect any Fe(III) (Fig. 6). Using the > 295 nm filter, [Fe]/[Na] decreased dramatically, and the pH fell over 3 units. Fe(III) was detected with thiocyanate. Fine orange particles were observed in the reactor.

Finally, when the full spectrum of the Hg lamp was used—with no filter—Fe precipitation continued. Thiocyanate showed an increase in [Fe(III)]. When the light was turned off, Fe precipitation stopped and pH increased slightly. The quantum yield calculated for < 345 nm was 0.08 ± 0.04.

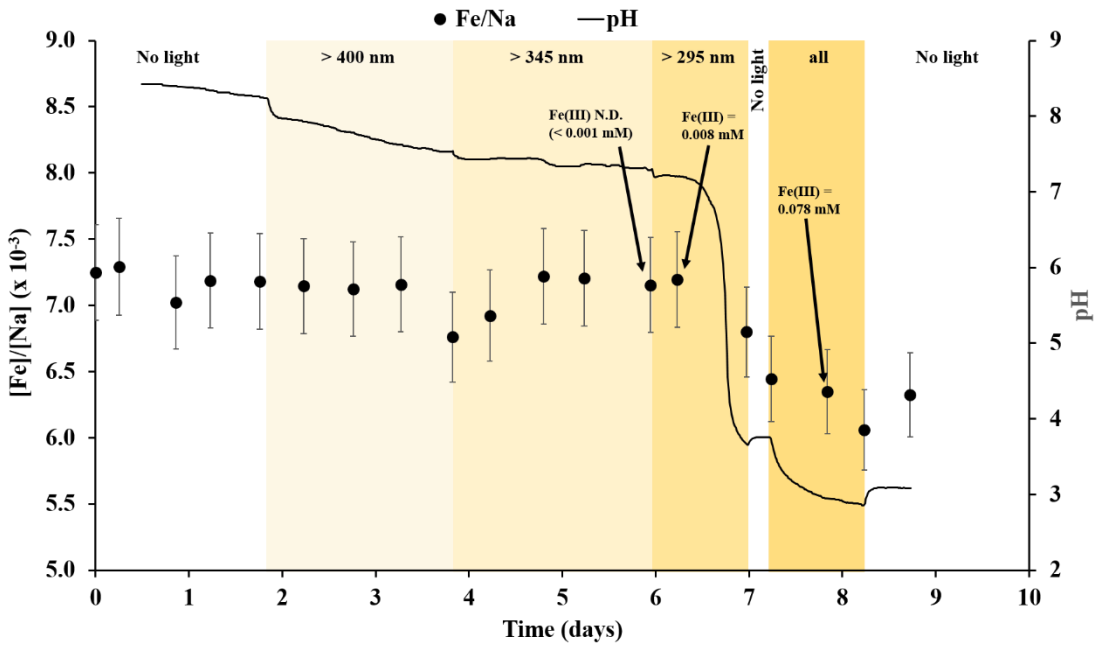


Figure 6. pH (black line) and [Fe]/[Na] data from the experiment attempting to replicate previous work. Note the pH changes right after changing filters. The short period where pH leveled off after day 7 was when the light was turned off for a brief period. The arrows and Fe(III) measurements indicate thiocyanate measurements of Fe(III) at the indicated time points. Error bars are ±5% of each value, estimated from repeated measurements of Fe and Na standards.

### 3.1.2 No Fe Control

During the experiment replicating the solution composition of previous work, but with no added Fe, the pH fell when the lamp was turned on (Fig. 7). It increased when the lamp was turned off.

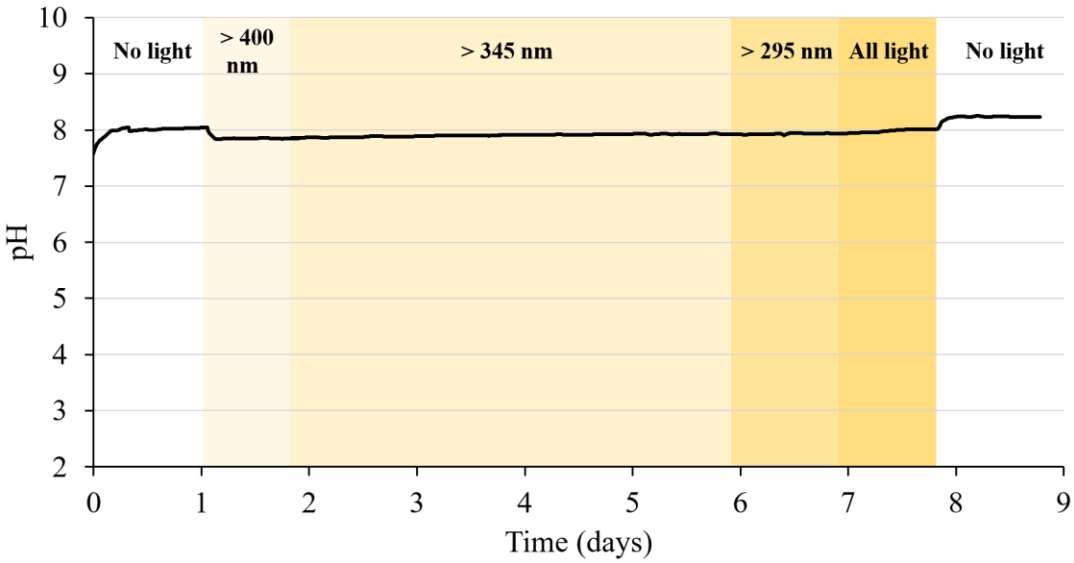


Figure 7. pH data from wavelength filter experiment with no added Fe. In this experiment pH dropped after the light was turned on, but didn't dramatically change when filters were changed. The pH drift was slight—only 0.2 units over 7 days. As observed in the previous experiment, pH increased when the light was turned off.

### 3.1.3 Testing Wavelength Dependence in a Realistic Solution

Using an Hg lamp with a bicarbonate-buffered solution, light > 400 nm was ineffective at causing Fe precipitation or oxidation (Fig. 8). Light > 345 nm also had no effect. Increasing the wavelength range to include light > 295 nm caused significant Fe oxidation and precipitation, with [Fe]/[Na] decreasing by 14% over 2 days. Orange

particles were observed in the vessel. Some were in suspension by the mixing and some settled to the bottom of the reactor. The full Hg lamp spectrum did not cause a major increase in precipitation rate. These results indicate Fe photooxidation is not caused by wavelengths > 345 nm. Using the decrease in [Fe] over the period with all wavelengths and the photon flux < 345 nm, we calculated an average quantum yield for wavelengths < 345 nm to be 0.03 ± 0.01 (see Appendix C for more details on how quantum yields were calculated).

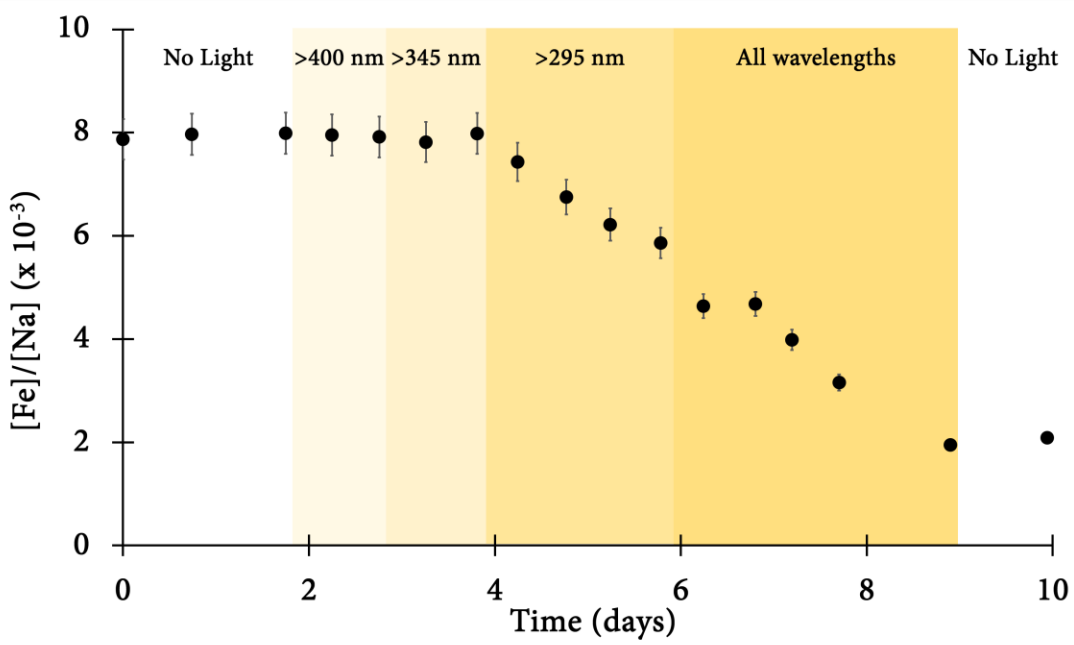


Figure 8. [Fe]/[Na] for wavelength cutoff filter experiment in a bicarbonate buffered solution. The [Fe]/[Na] does not change even with light > 345 nm, but decreases after light between 345 and 295 nm is included. When the light is turned off, [Fe]/[Na] ceases to decrease, indicating Fe precipitation stopped. Error bars are ±5% of each value, estimated from repeated measurements of Fe and Na standards.

### 3.1.4 Testing Photooxidation in a Realistic Setting – Xe Lamp Experiments

Using the AM0 filter, the Xe lamp showed no Fe precipitation or oxidation. When the filter was removed, there was a moderate decrease in [Fe]/[Na] (Fig. 9) and [Fe(II)] (Fig. 10). About 35% of the Fe precipitated in about 4.5 days. The rate was 0.013 mM Fe/day. Similar to the Hg lamp experiments, orange particles were noted in suspension and at the bottom of the reactor. The average quantum yield for the unfiltered Xe lamp for wavelengths < 345 nm was calculated to be 0.04 ± 0.01.

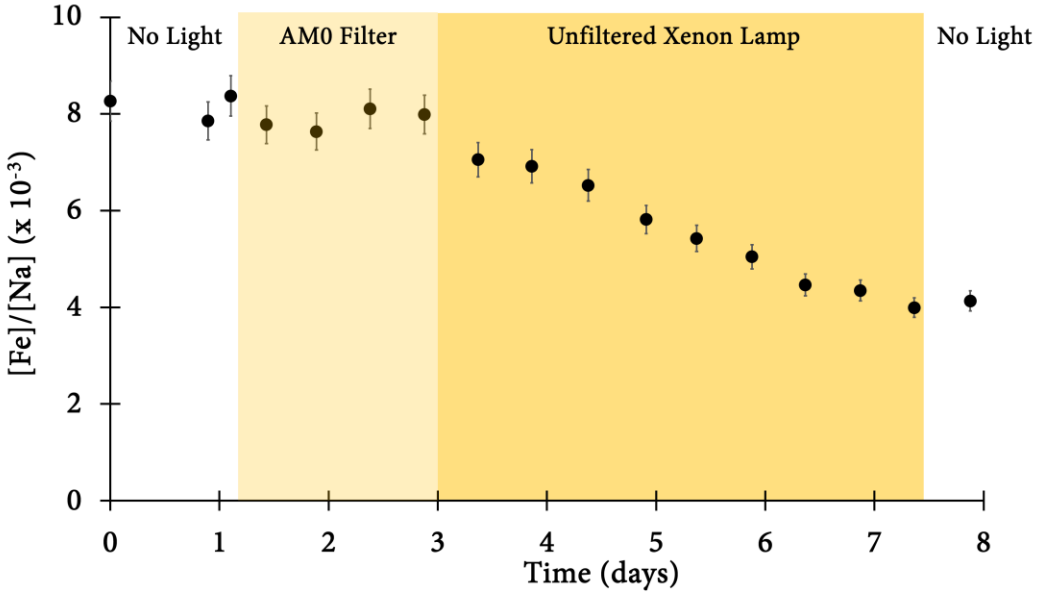


Figure 9. [Fe]/[Na] for the experiment using a Xe lamp and a bicarbonate buffered solution. Even when the lamp is turned on, the [Fe]/[Na] ratio does not decrease until the solar simulator filter is removed. Error bars are ±5% of each value, estimated from repeated measurements of Fe and Na standards.

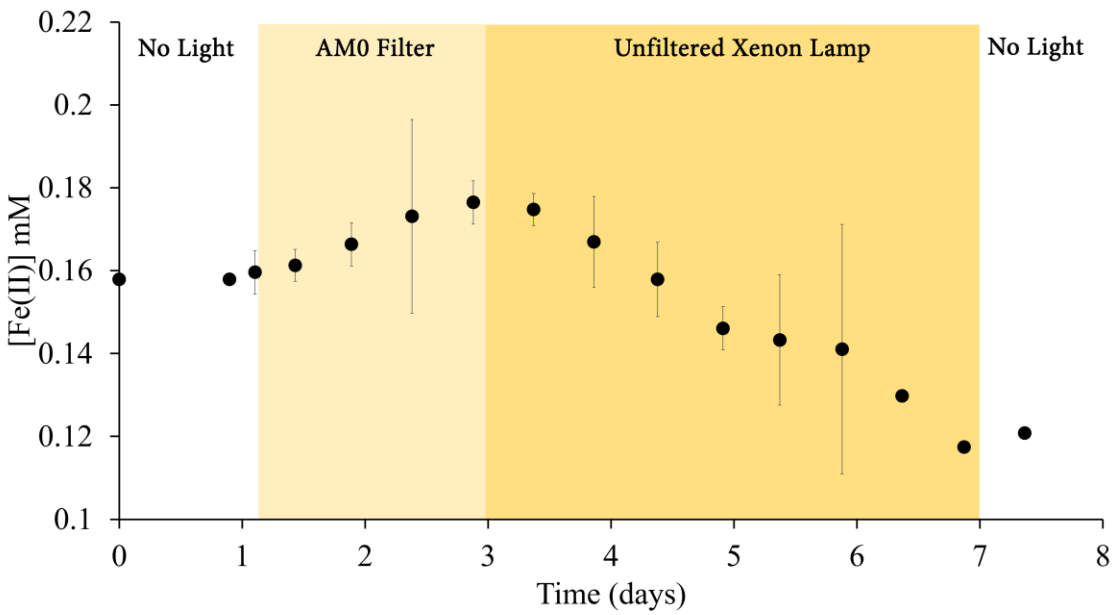


Figure 10. [Fe(II)], determined using the ferrozine method, for the experiment using a Xe lamp and a bicarbonate buffered solution. These data show the same trend as for total [Fe]/[Na]. The increase in the beginning periods, before the AM0 filter was removed, is likely due to evaporation. Error bars are ±2σ of triplicate cuvette measurements.

### 3.1.5 Precipitate Analysis

Raman analysis of the orange particles gave a spectrum most consistent with Lepidocrocite (γ-FeO(OH)) (Fig. 11). A peak at Raman shift 528 $cm^{-1}$ was much lower in the sample than in the database reference spectrum.

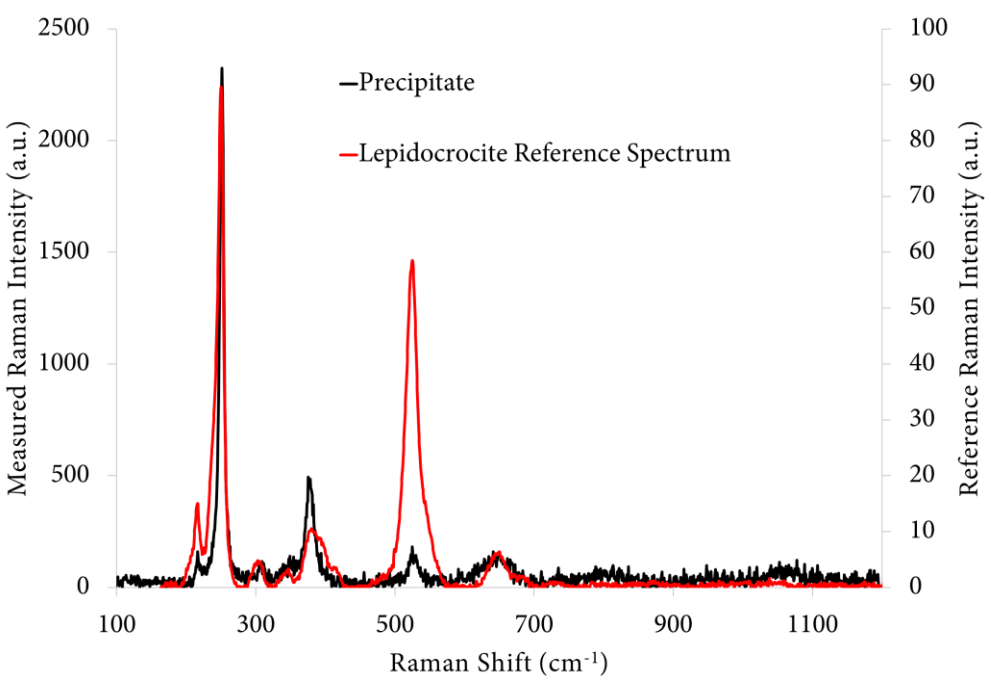


Figure 11. Raman spectrum of recovered precipitates. The precipitate generally matches Lepidocrocite (γ-FeO(OH)). There is a difference in one peak intensity, which is discussed below.

### 3.1.6 Actinometry Results

Overall photon flux in the UV using the 2-nitrobenzaldehyde actinometer (Allen et al., 2000) was determined to be $2.4 \times 10^{-6}$ mol photons $s^{-1}$ for the Hg lamp and $0.87 \times 10^{-6}$ mol photons $s^{-1}$ for the unfiltered Xe lamp.

## 3.2 Modeling Results

Replicating the ocean photooxidation model of Francois (1986), calculating Fe photooxidation rate as a function of seawater [Fe(II)], created a curve that matched the

calculations of Francois (1986) (Fig. 12). Following the results of Braterman et al (1983), this calculation assumed wavelengths as long as 460 nm caused photooxidation.

However, if we limit the reaction to the wavelength region found important in our experiments (< 345 nm), we find BIF mass accumulation rates 5 to 6 times slower. At the upper limit of Archean seawater [Fe(II)] (0.18 mM) (Holland, 1973), BIF mass accumulation rates are calculated as 19 mg Fe $cm^{-2}$ $yr^{-1}$ (Fig. 12).

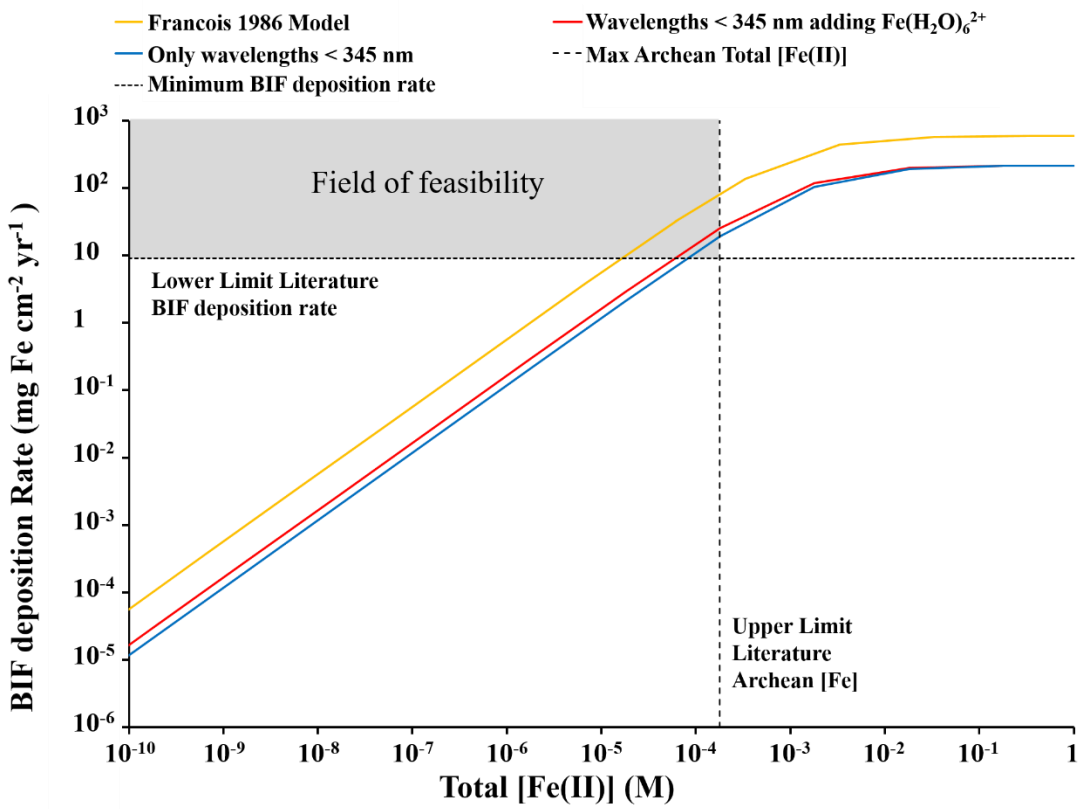


Figure 12. BIF deposition rate as a function of seawater [Fe(II)] for Francois (1986) and our models. Our modeled Fe deposition rates are significantly lower than previous models, only narrowly overlapping the field of feasibility.

Adding in the photooxidation of $Fe(H_2O)_6^{2+}$ into the model, calculated BIF deposition rates increase to 25 mg Fe $cm^{-2}$ $yr^{-1}$ (Fig. 12). $Fe(H_2O)_6^{2+}$ photooxidation at short wavelengths has been well documented (Rigg and Weiss, 1952).

# CHAPTER 4 DISCUSSION

## 4.1 Experiments

### 4.1.1 Reevaluation of Previous Work

The experiment to resolve the discrepancy in results between Braterman et al. (1983) and Konhauser et al. (2007) showed no Fe precipitation with light > 400 nm or > 345 nm. Light > 295 nm was effective in causing photooxidation. This result disagrees with Braterman et al. (1983)'s observation that light > 400 nm was effective, and is not inconsistent with Konhauser et al. (2007). Braterman et al. (1983) mainly inferred photooxidation by pH change. The pH did decrease when the solution was irradiated with > 400 nm light, however this change of about 0.2 units is much smaller than Braterman et al. (1983) observed. Konhauser et al. (2007) noted their solution pH decreased by "less than 1 unit" when irradiated with 320 – 400 nm light, suggesting they observed a light-pH effect similar to ours. The reason for this small pH change was potentially clarified in an experiment with the same solution but no added Fe, where pH changed when the light was turned on. Light > 295 nm caused a large pH decrease. This large decrease is expected when Fe oxidizes and precipitates.

Braterman et al. (1983) reported that photooxidation of Fe with light > 366 nm caused the appearance of Fe(III) as measured by thiocyanate. However, using thiocyanate we did not detect any Fe(III) after the > 400 nm and > 345 nm filters (< 0.001 mM). If our Fe was indeed photooxidized but did not precipitate or formed particles < 0.2 μm, we would expect to detect Fe(III) with thiocyanate. After a period of light > 295 nm where we observed Fe precipitation and a large pH decrease, thiocyanate did detect Fe(III).

Using the lower limit $Fe(OH)^+$ quantum yield Braterman et al. (1983) calculated of 0.01 for 366 nm and the light flux of our lamp, we can calculate the expected decrease in [Fe] (and using measured decreases in [Na] the expected decrease in [Fe]/[Na]) if photooxidation did indeed occur with light > 400 nm or > 345 nm. This calculated theoretical decrease in [Fe]/[Na] is $3x10^{-3}$. This is far larger than either uncertainty in the linear regression ($\pm 4.1x10^{-5}$) and analytical uncertainties in the measurements (about $\pm 3.6x10^{-4}$). This means that if the quantum yield determined by Braterman et al. (1983) is correct, then we would have measured the Fe precipitation.

Braterman added his Fe(II) as $Fe(SO_4)(s)$ while we used $FeCl_2$, however we do not expect this to make a difference as $FeCl^+$ and $Fe(SO_4)(aq)$ do not absorb light > 350 nm. Thermodynamic calculations show $[Fe(OH)^+]$ does not change significantly (< 10%) between the two solutions.

We can only speculate as to why Braterman et al. (1983) observed photooxidation at long wavelengths while we and Konhauser et al. (2007) did not. One possibility is that Braterman observed short-wave visible or long-wave UV light reacting with organic compounds in the solution in a way that lowered pH. Organics may also be the cause of the slow pH drift downward in our experiment.

### 4.1.2 No Fe Control

The experiment with no added Fe showed pH decreasing about 0.2 units with light and increasing again when the light was turned off. This suggests that the small pH changes we observed were an effect of the light, but not due to Fe photooxidation. One possibility is heating by the light. Direct heating of the solution is not likely because

while pH is sensitive to temperature, a change of 0.2 units at pH ~8 would require heating the solution from about 25 °C to about 80 °C. As our experiment was kept in a fume hood, there was constant airflow to help maintain the temperature of the reactor. Though the exact temperature was never measured, the reactor never got hot to the touch. On the other hand, it is possible the light affects the temperature of the pH probe itself. Because the pH probe has dark coloration, that material could have been heated, causing a temperature effect without heating the entire experimental solution. Organic compounds reacting in the solution are an unlikely cause of the pH changes, as this experiment used HPLC grade water (the previous experiment did not).

### 4.1.3 Testing Wavelength Dependence in a Realistic Solution

The results of the realistic (i.e. bicarbonate buffered) solution were similar to the experiment retesting previous work. No Fe photooxidation or precipitation were observed with light > 345 nm, while light > 295 nm caused Fe oxidation and precipitation. $Fe(H_2O)_6^{2+}$ has absorbance < 300 nm (Fig. 12), so it would absorb a small amount of light

(a range of about 5 nm) from this filter region.

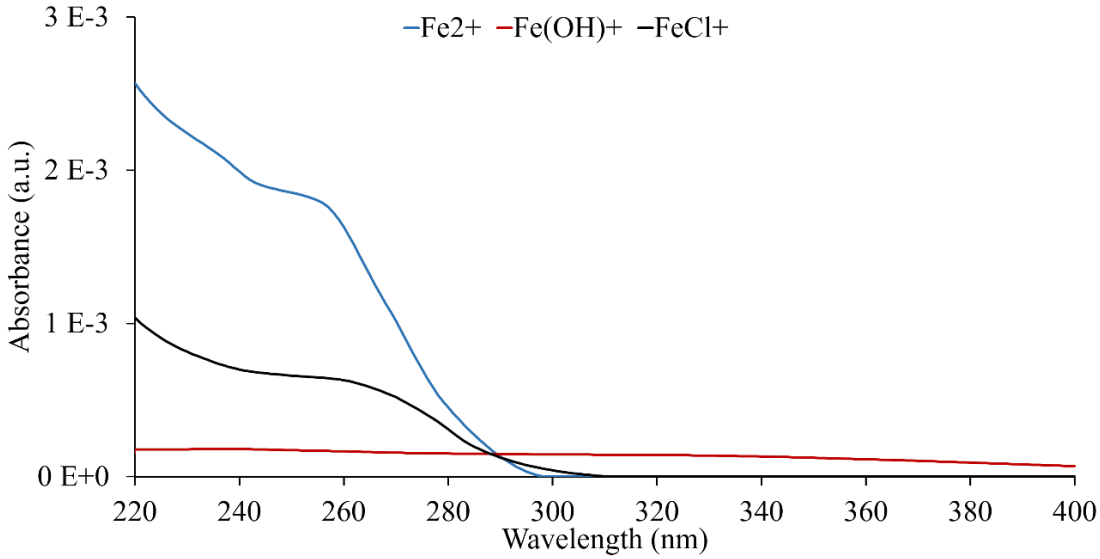


Figure 13. Modeled absorbances of Fe species with known absorbance spectra in our bicarbonate buffered solution. Though lower in molar absorptivity (see Fig. 2) $Fe(H_2O)_6^{2+}$ and $FeCl^+$ dominate the spectrum < 290 nm because they are more abundant in solution compared to $Fe(OH)^+$ (60%, 10%, and 0.26% of all Fe(II) respectively).

However, to fully explain the photooxidation we observed for this filter, it would require a quantum yield for $Fe(H_2O)_6^{2+}$ photooxidation over 1, which is not possible. The quantum yield for $Fe(H_2O)_6^{2+}$ photooxidation has been experimentally determined to be 0.14 (Rigg and Weiss, 1952). Furthermore, $Fe(H_2O)_6^{2+}$ absorbs most strongly at shorter wavelengths and the Hg lamp irradiance is < 295 nm is twice that of between 295 and 300 nm, so if $Fe(H_2O)_6^{2+}$ was exclusively responsible for the observed photooxidation, we would expect to have observed the photooxidation rate to increase dramatically when the >295 nm light filter was removed. Therefore, another Fe species must play a role. Braterman et al. (1983) attributed the long-wave UV photooxidation they observed to the

Fe(II) species $Fe(OH)^+$ because it absorbs at wavelengths from 200 to 450 nm. This species is still the best explanation for our observed photooxidation >295 nm. Reactions of $FeHCO_3^+$ and $FeCO_3$ cannot be ruled out, as spectra for these Fe(II) carbonate species have not been measured, but > 295 nm photooxidation also occurred in the unbuffered solution experiment without bicarbonate so Fe carbonates cannot be the only species reacting.

There is a notable limitation of this experiment. We observed no photooxidation > 345 nm but did using a filter > 295 nm. It is possible that the reaction is sensitive to only a portion of the 295 – 345 nm region. Konhauser et al. (2007)'s experiment with a UV floodlamp 320 – 400 nm showed no photooxidation, so it might be that the longest wavelength that photooxidizes Fe is 320 nm. However, the lamp used by Konhauser et al. (2007) is extremely faint in the range 320 – 400 nm, and they had no light in the range 256 – 320 nm. Their photon flux (after accounting for their area illuminated and path length, though not accounting for internal reflections in their set-up), is approximately an order of magnitude less than our experiment over the same wavelength range. Assuming $Fe(OH)^+$ is the absorbing species, even if it was photooxidized with a quantum yield of 1, the rate would be within their reported error. Our experiments can rule out wavelengths > 345 nm, cannot necessarily include 320 – 345 nm, and with such a low flux, Konhauser et al. (2007)'s results cannot not rule out 320 – 345 nm.

### 4.1.4 Testing Photooxidation in a Realistic Setting – Xe Lamp Experiments

The first interesting result of the Xe lamp experiment is how the lamp with AM0 filter did not cause precipitation while an unfiltered Xe lamp did. An explanation for this is the filter's large absorbance 295 – 350 nm—the wavelengths we identified to cause Fe photooxidation in the previous experiment. While the AM0 filter makes the Xe lamp better match the solar spectrum > 350 nm, the unfiltered Xe lamp better matches the solar spectrum 295 – 350 nm. An experiment using the Xe lamp, with realistic solar flux, spectrum, realistic [Fe(II)], and a bicarbonate buffered solution showed significant precipitation in hours. A fainter Archean sun would slow this rate, but only by 20-30% (Claire et al., 2012)

### 4.1.5 Precipitate Analysis

The precipitate Raman spectrum matched closely with the Fe oxyhydroxide Lepidocrocite (γ-FeO(OH)). This is consistent with the results of Anbar and Holland (1992), measured by X-ray diffraction. The Raman spectrum in the sample lacks the Raman peak at about 528 $cm^{-1}$ in the RRUFF database's Lepidocrocite reference spectrum (Bindi et al., 2016). However, other published Lepidocrocite Raman spectra have a fainter peak, better matching our sample (Hanesch, 2009). This discrepancy is possibly because the spectrum in the database is for a natural mineral sample, while the Hanesch (2009) spectrum is from synthetic Lepidocrocite.

## 4.2 Model Discussion

### 4.2.1 Comparison to Other Fe Oxidation Rates

Our modeled Fe photooxidation rate of 25 mg Fe $cm^{-2}$ $yr^{-1}$ is within the low end of geological estimates for BIF deposition, 9 – 43 mg Fe $cm^{-2}$ $yr^{-1}$ (Trendall and Blockley, 1970) , but is considerably lower than higher estimates 254 mg Fe $cm^{-2}$ $yr^{-1}$ (Konhauser et al., 2002). These rates, however, are for the late Archean Hamersley Basin BIF—one of the largest, best preserved and most well studied BIFs. Other BIFs may have been deposited slower though their deposition rates are poorly constrained (Bekker et al., 2010).

Our calculated Fe photooxidation rates are far slower than Fe oxidation rates calculated for a community of photoferrotrophs in the ocean. Models can give Fe oxidation rates above 500 mg Fe $cm^{-2}$ $yr^{-1}$ (Kappler et al., 2005), an order of magnitude higher than Fe photooxidation rates for similar [Fe(II)].

### 4.2.2 Model Assumptions and Limitations

One important model input is the longest wavelength causing photooxidation. We limited our models to < 345 nm to calculate an upper limit on the rate. However, if no photooxidation occurs with light > 320 nm as Konhauser et al. (2007) observed, Fe oxidation rates in our model are reduced by about 1/3 to 19 mg Fe $cm^{-2}$ $yr^{-1}$. This is still greater than 9 mg Fe $cm^{-2}$ $yr^{-1}$, but this slower rate is combined with other possible factor slowing photooxidation might make photooxidation too slow to deposit BIFs. More

experiments, using a greater number of cutoff filters or even a laser that scans wavelengths (if intense enough) are needed to narrow down the range.

Our model itself makes several notable favorable assumptions: 1) a well-mixed ocean bringing continuous supply of Fe(II) to surface and homogenizing [Fe(II)] 2) Fe precipitates sink instantly so they do not attenuate light 3) no light attenuation of the Archean atmosphere between 200 and 345 nm.

The assumption that light attenuation by Fe precipitates can be ignored because they sink instantly is questionable. If the ocean is well mixed enough to have a continuous supply of Fe(II) brought to the surface and homogeneous [Fe(II)], the mixing could suspend some Fe particles as they grow. Empirically, in our experiments while most Fe precipitates seemed to sink to the reactor bottom, some particles were suspended. The attenuation of these particles should be measured and accounted for in future models.

The Archean atmosphere is a factor not fully accounted for. Our model assumed no attenuation between 200 and 345 nm. However, there was likely some attenuation in the UV (from $H_2S$, $SO_4$, aerosols, and potentially organic hazes), but the exact magnitude and wavelengths of this attenuation is an open question (Ranjan and Sasselov, 2016).

Another consideration for accurate photochemical modeling is the Fe species being photooxidized. We included $Fe(OH)^+$ and $Fe(H_2O)_6^{2+}$ in our models. However, other Fe(II) species may be photooxidized. $FeCl^+$ is a major species in high $Cl^-$ solutions and has moderate UV absorbance < 295 nm (Fig. 2). However, it would contribute little to the overall photooxidation rate (Fig. 14), assuming its quantum yield is similar to $Fe(H_2O)_6^{2+}$.

Photooxidation of $Fe(SO_4)$ could be possible. It has absorbance into the mid-UV, up to 350 nm (Fig. 2), so it might be significant because of increased solar photon flux and more transparent seawater vs short-wave UV at those wavelengths. However, the Archean ocean is thought to have low (< 2.5 μM) sulfate concentrations (Crowe et al., 2014). In our model, the contribution to overall Fe photooxidation rates from $Fe(SO_4)$ is negligible. Even increasing the quantum yield to 1, the contribution from photooxidation of $Fe(SO_4)$ is still very minor in comparison to other Fe species (Fig. 14).

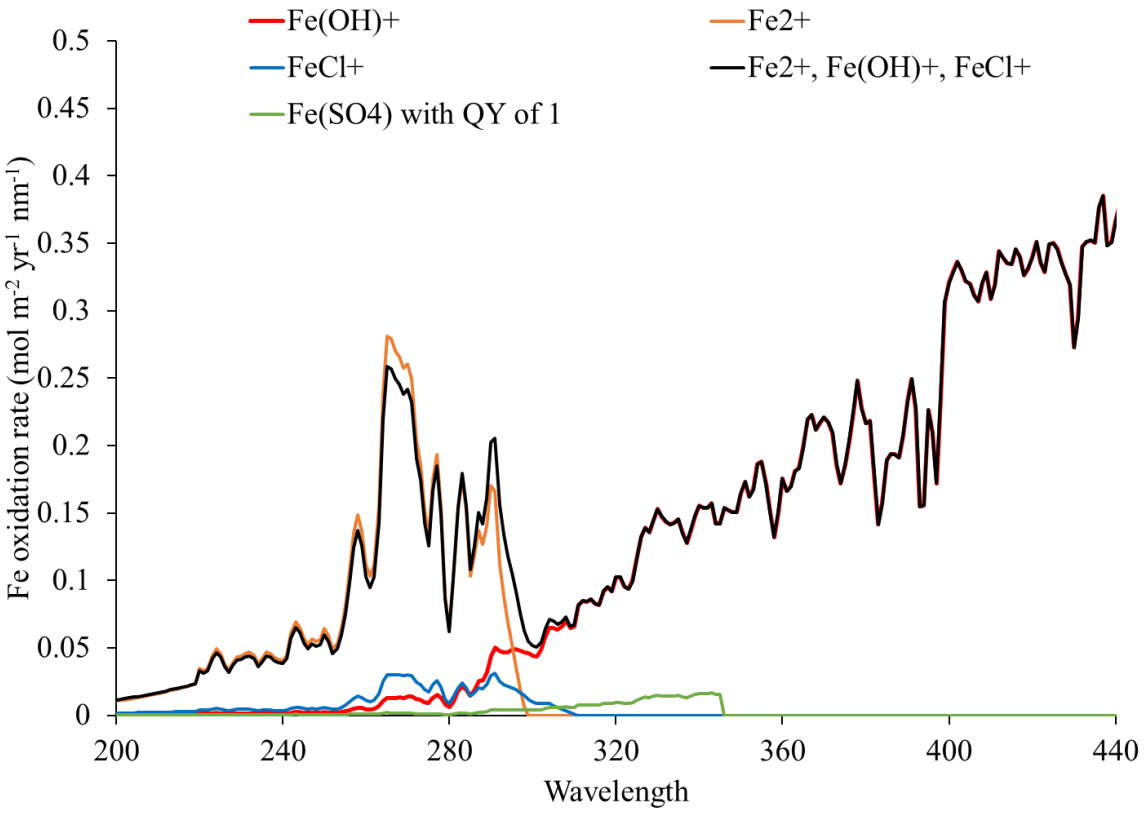


Figure 14. Calculated Fe photooxidation rate as a function of wavelength for models with different Fe(II) species. Water total [Fe(II)] = 0.18 mM. QY = quantum yield. $Fe(OH)^+$ is entirely responsible for photooxidation at long wavelengths. While $Fe(OH)^+$ and

$Fe(H_2O)_6^{2+}$ absorption continue to strengthen at decreasing wavelengths, the solar spectrum has less irradiance, causing lower photooxidation rates.

The potential role of Fe(II) bicarbonate and carbonate ($FeHCO_3^+$ and $FeCO_3$) could not be evaluated as no published UV-VIS absorbance spectra for those species exist. Future work should measure the spectra of these major species.

### 4.2.3 Other Considerations

While our bicarbonate buffered solution is a major improvement on previous work, it still lacks many components found in natural seawater that might impact the reaction. Ions in solution such as $Ca^{2+}$ and $Mg^{2+}$ would affect Fe speciation. Other components such as $I^-$ and organic carbon have UV absorbance that could shield Fe (Murov et al., 1993). More interestingly, Mn itself can be photooxidized and could react with Fe (Anbar and Holland, 1992). Reactions between dissolved organic carbon (DOC) and Fe photochemistry have been documented modern systems and the subject of ongoing study (e.g. Faust and Zepp, 1993; Garg et al., 2015; Miller et al., 1995). A process common in natural waters today is Fe photoreduction by oxidation of organic matter (Garg et al., 2015) so if DOC is present Fe photoreduction might occur and re-reduce any Fe photooxidized.

# CHAPTER 5 CONCLUSIONS AND IMPLICATIONS

## 5.1 Conclusions

Our objectives were to test BIF deposition by Fe photooxidation by reevaluating previous work, then extending experiments into more realistic conditions. By replicating the solution of previous works and using a similar light source, we did not observe > 400 nm photooxidation reported in Braterman et al. (1983). We found Fe photooxidation does not occur with light > 345 nm, but does with light > 295 nm. The same wavelength dependence was found in a more realistic bicarbonate buffered solution. As these wavelengths are too long for $Fe(H_2O)_6^{2+}$, $Fe(OH)^+$ is likely the absorbing species in addition to $Fe(H_2O)_6^{2+}$. An experiment using the Xe lamp showed measurable effects in hours, demonstrating the potential for Fe to photooxidize significantly in a natural environment.

To calculate if Fe photooxidation is rapid enough to deposit BIFs, we built a model based on previous work (François, 1986). We improved it by considering other Fe species that could be photooxidized in addition to $Fe(OH)^+$. Adding $Fe(H_2O)_6^{2+}$ had a large effect on the overall rate, while $FeCl^+$ and $Fe(SO_4)$ were minor. Using this model, assuming [Fe(II)] at the upper limit for Archean seawater [Fe(II)] (Holland, 1973), we calculate BIF deposition rates of 25 mg Fe $cm^{-2}$ $yr^{-1}$. This number is within the range of conservative BIF deposition rate estimates of 9 - 43 mg $cm^{-2}$ $yr^{-1}$ (Trendall and Blockley, 1970), but far less than the largest estimates of 254 mg $cm^{-2}$ $yr^{-1}$ (Konhauser et al., 2002). Our model has favorable assumptions such as no light attenuation 200 - 400 nm by the

Archean atmosphere or Fe particles in suspension. Because our calculated Fe deposition rates are close to lower estimates of natural rates, these assumptions should be investigated and accounted for in future work. Additionally, ocean constituents such as Mn and DOC that could undergo photochemistry, could react with Fe, and block light, should be evaluated experimentally and added into models. BIF sedimentation rate estimates are for one of the largest BIFs, so even if photochemistry is too slow to fully account for that particular BIF, other BIFs with unconstrained deposition rates cannot be excluded.

### 5.2 Implications

Though it appears photooxidation is barely able to account for BIF deposition under favorable conditions, Fe can photooxidize under realistic conditions in hours as shown in our Xe lamp experiment. Fe photooxidation could have been an important background process pervasive in shallow-water environments such as lakes, rivers, or the open ocean, not subject to biological limits such as nutrient availably or protection from surface UV. Unlike microbial processes which require the necessary metabolism to evolve, photooxidation could take place throughout Earth's history. For example, this Fe oxidation might impact Archean ocean global Mo budgets. Future work should quantify the significance of this background process.

Thinking beyond Fe, this work demonstrates UV light has significant oxidizing power over short timescales. In the Archean, UV light could impact paleoredox proxies that rely on a redox sensitive metal or mineral, such as the Cr isotope proxy requiring Mn

oxides (Planavsky et al., 2014). Especially if these proxies are to be used quantitatively, the influence of UV light must be quantified.

# REFERENCES


Allen, J. M.; Allen, S. K.; Baertschi, S. W. 2-Nitrobenzaldehyde: a convenient UV-A and UV-B chemical actinometer for drug photostability testing. *J. Pharm. Biomed. Anal.* **2000**, *24*, 167-178.

Anbar, A.; Holland, H. The photochemistry of manganese and the origin of banded iron formations. *Geochim. Cosmochim. Acta* **1992**, *56*, 2595-2603.

Anbar, A. D.; Duan, Y.; Lyons, T. W.; Arnold, G. L.; Kendall, B.; Creaser, R. A.; Kaufman, A. J.; Gordon, G. W.; Scott, C.; Garvin, J.; Buick, R. A Whiff of Oxygen Before the Great Oxidation Event? *Science* **2007**, *317*, 1903-1906.

Bekker, A.; Slack, J. F.; Planavsky, N.; Krapez, B.; Hofmann, A.; Konhauser, K. O.; Rouxel, O. J. Iron Formation: The Sedimentary Product of a Complex Interplay among Mantle, Tectonic, Oceanic, and Biospheric Processes*. *Economic Geology* **2010**, *105*, 467.

Bindi, L.; Churakov, S. V.; Downs, R.; Gfeller, F.; Krivovichev, S. V.; Lafuente, B.; Mugnaioli, E.; Nestola, F.; Steinhardt, P. J.; Stone, N. *Highlights in Mineralogical Crystallography;* Walter de Gruyter GmbH & Co KG: 2016; .

Braterman, P. S.; Cairns-Smith, A.; Sloper, R. W. Photo-oxidation of hydrated Fe2+—significance for banded iron formations. *Nature* **1983**, *303*, 163-164.

Cairns-Smith, A. Precambrian solution photochemistry, inverse segregation, and banded iron formations. *Nature* **1978**, *276*, 807-808.

Claire, M. W.; Sheets, J.; Cohen, M.; Ribas, I.; Meadows, V. S.; Catling, D. C. The evolution of solar flux from 0.1 nm to 160 μm: quantitative estimates for planetary studies. *Astrophys. J.* **2012**, *757*, 95.

Cloud, P. Paleoecological significance of the banded iron-formation. *Economic Geology* **1973**, *68*, 1135-1143.

Crowe, S. A.; Paris, G.; Katsev, S.; Jones, C.; Kim, S.; Zerkle, A. L.; Nomosatryo, S.; Fowle, D. A.; Adkins, J. F.; Sessions, A. L.; Farquhar, J.; Canfield, D. E. Sulfate was a trace constituent of Archean seawater. *Science* **2014**, *346*, 735-739.

Downs, R. In *In The RRUFF Project: an integrated study of the chemistry, crystallography, Raman and infrared spectroscopy of minerals;* Program and abstracts of the 19th general meeting of the international mineralogical association in Kobe, Japan; 2006; Vol. 3, pp 13.

Ehrenfreund, M.; Leibenguth, J. Etude des équilibres d'hydrolyse des ions de Fe (II) par spectrophotométrie ultra-violette et visible. II.—Etude en milieu (NH4) 2SO4–2M, ou NaClO4–2M. Essai d'interpretation. *Bulletin de la Société Chimique de France* **1970**, *7*, 2498-2505.

Farquhar, J.; Bao, H.; Thiemens, M. Atmospheric Influence of Earth's Earliest Sulfur Cycle. *Science* **2000**, *289*, 756-758.

Faust, B. C.; Zepp, R. G. Photochemistry of aqueous iron (III)-polycarboxylate complexes: roles in the chemistry of atmospheric and surface waters. *Environ. Sci. Technol.* **1993**, *27*, 2517-2522.

François, L. M. Extensive deposition of banded iron formations was possible without photosynthesis. **1986**.

Garg, S.; Jiang, C.; Waite, T. D. Mechanistic insights into iron redox transformations in the presence of natural organic matter: Impact of pH and light. *Geochim. Cosmochim. Acta* **2015**, *165*, 14-34.

Gran, G. Determination of the Equivalence Point in Potentiometric Titrations. Part II. *The Analyst* **1952**, *77*, 661-671.

Gueymard, C.; Myers, D.; Emery, K. Proposed reference irradiance spectra for solar energy systems testing. *Solar Energy* **2002**, *73*, 443-467.

Hanesch, M. Raman spectroscopy of iron oxides and (oxy) hydroxides at low laser power and possible applications in environmental magnetic studies. *Geophysical Journal International* **2009**, *177*, 941-948.

Heinrich, C.; Seward, T. A spectrophotometric study of aqueous iron (II) chloride complexing from 25 to 200 C. *Geochim. Cosmochim. Acta* **1990**, *54*, 2207-2221.

Hessler, A. M.; Lowe, D. R.; Jones, R. L.; Bird, D. K. A lower limit for atmospheric carbon dioxide levels 3.2 billion years ago. *Nature* **2004**, *428*, 736-738.

Holland, H. D. The oceans; a possible source of iron in iron-formations. *Economic Geology* **1973**, *68*, 1169-1172.

Holland, H. D.; Schidlowski, M. *Mineral Deposits and the Evolution of the Biosphere;* Springer: 1982; .

Kappler, A.; Pasquero, C.; Konhauser, K. O.; Newman, D. K. Deposition of banded iron formations by anoxygenic phototrophic Fe (II)-oxidizing bacteria. *Geology* **2005**, *33*, 865-868.

Kasting, J. F.; Donahue, T. The evolution of atmospheric ozone. *Journal of Geophysical Research: Oceans* **1980**, *85*, 3255-3263.

Konhauser, K. O.; Amskold, L.; Lalonde, S. V.; Posth, N. R.; Kappler, A.; Anbar, A. Decoupling photochemical Fe (II) oxidation from shallow-water BIF deposition. *Earth Planet. Sci. Lett.* **2007**, *258*, 87-100.

Konhauser, K. O.; Hamade, T.; Raiswell, R.; Morris, R. C.; Ferris, F. G.; Southam, G.; Canfield, D. E. Could bacteria have formed the Precambrian banded iron formations? *Geology* **2002**, *30*, 1079-1082.

Laetsch, T.; Downs, R. In *In Software for identification and refinement of cell parameters from powder diffraction data of minerals using the RRUFF Project and American Mineralogist Crystal Structure Databases;* 19th General Meeting of the International Mineralogical Association, Kobe, Japan; 2006; Vol. 23, pp e28.

Lide, D. R. *CRC handbook of chemistry and physics;* CRC press: 2004; .

Luo, G.; Ono, S.; Beukes, N. J.; Wang, D. T.; Xie, S.; Summons, R. E. Rapid oxygenation of Earth's atmosphere 2.33 billion years ago. *Sci Adv* **2016**, *2*.

Lyons, T. W.; Reinhard, C. T.; Planavsky, N. J. The rise of oxygen in Earth/'s early ocean and atmosphere. *Nature* **2014**, *506*, 307-315.

Matson, R. J.; Emery, K. A.; Bird, R. E. Terrestrial solar spectra, solar simulation and solar cell short-circuit current calibration: a review. *Solar Cells* **1984**, *11*, 105-145.

Miller, W. L.; King, D. W.; Lin, J.; Kester, D. R. Photochemical redox cycling of iron in coastal seawater. *Mar. Chem.* **1995**, *50*, 63-77.

Murov, S. L.; Carmichael, I.; Hug, G. L. *Handbook of photochemistry;* CRC Press: 1993; .

Parkhurst, D. L.; Appelo, C. *Description of input and examples for PHREEQC version 3: a computer program for speciation, batch-reaction, one-dimensional transport, and inverse geochemical calculations* **2013**.

Planavsky, N. J.; Asael, D.; Hofmann, A.; Reinhard, C. T.; Lalonde, S. V.; Knudsen, A.; Wang, X.; Ossa, F. O.; Pecoits, E.; Smith, A. J. Evidence for oxygenic photosynthesis half a billion years before the Great Oxidation Event. *Nature geoscience* **2014**, *7*, 283-286.

Potterill, R.; Walker, O.; Weiss, J. Electron affinity spectrum of ferrous ion in aqueous solution. *Proceedings of the Royal Society of London.Series A, Mathematical and Physical Sciences* **1936**, *156*, 561-570.

Ranjan, S.; Sasselov, D. D. Influence of the UV Environment on the Synthesis of Prebiotic Molecules. *Astrobiology* **2016**, *16*, 68-88.

Rigg, T.; Weiss, J. Photochemistry of ferrous ions in aqueous solution. *J. Chem. Phys.* **1952**, *20*, 1194-1199.

Sandell, E. B. *Colorimetric determination of traces of metals;* Interscience Publishers: New York: 1950; .

Smith, R. C.; Baker, K. S. Optical properties of the clearest natural waters (200–800 nm). *Appl. Opt.* **1981**, *20*, 177-184.

Stookey, L. L. Ferrozine---a new spectrophotometric reagent for iron. *Anal. Chem.* **1970**, *42*, 779-781.

Tedetti, M.; Sempéré, R. Penetration of ultraviolet radiation in the marine environment. A review. *Photochem. Photobiol.* **2006**, *82*, 389-397.

Trendall, A.; Blockley, J. The iron formations of the Hamersley Group, Western Australia, with special reference to the associated crocidolite. *Western Austr.Surv.Bull* **1970**, *119*, 353.

# APPENDIX A

# EXPERIMENTAL DATA

Table 2. [Fe]/[Na] of the experiment reevaluating previous results

| Sample No. | Time (days) | [Fe]/[Na] |
|---|---|---|
| 1 | 0.00 | 0.007249 |
| 2 | 0.25 | 0.007292 |
| 3 | 0.86 | 0.007022 |
| 4 | 1.23 | 0.007188 |
| 5 | 1.76 | 0.007181 |
| 6 | 2.23 | 0.007146 |
| 7 | 2.76 | 0.007122 |
| 8 | 3.27 | 0.007158 |
| 9 | 3.82 | 0.006760 |
| 10 | 4.22 | 0.006923 |
| 11 | 4.80 | 0.007220 |
| 12 | 5.23 | 0.007205 |
| 13 | 5.95 | 0.00715 |
| 14 | 6.23 | 0.007196 |
| 15 | 6.97 | 0.00679899 |
| 16 | 7.24 | 0.006442641 |
| 17 | 7.84 | 0.006348464 |
| 18 | 8.23 | 0.006059215 |
| 19 | 8.72 | 0.006323407 |

Table 3. [Fe]/[Na] of the experiment testing wavelength dependence in a bicarbonate buffered solution

| Sample No. | Time (days) | [Fe]/[Na] |
|---|---|---|
| 1 | 0.00 | 0.0003233 |
| 2 | 0.74 | 0.0003273 |
| 3 | 1.75 | 0.0003281 |
| 4 | 2.25 | 0.0003266 |
| 5 | 2.76 | 0.0003252 |
| 6 | 3.26 | 0.0003210 |
| 7 | 3.81 | 0.0003280 |
| 8 | 4.24 | 0.0003053 |
| 9 | 4.77 | 0.0002774 |
| 10 | 5.24 | 0.0002554 |
| 11 | 5.78 | 0.0002407 |
| 12 | 6.24 | 0.0001905 |
| 13 | 6.80 | 0.0001921 |
| 14 | 7.20 | 0.0001637 |
| 15 | 7.70 | 0.0001296 |
| 16 | 8.90 | 0.0000801 |
| 17 | 9.94 | 0.0000857 |

Table 4. [Fe]/[Na] of the experiment testing photooxidation using a Xe lamp

| Sample No. | Time (days) | [Fe]/[Na] |
|---|---|---|
| 1 | 0.00 | 0.0003148 |
| 2 | 0.90 | 0.0002811 |
| 3 | 1.10 | 0.0003107 |
| 4 | 1.43 | 0.0002932 |
| 5 | 1.89 | 0.0002574 |
| 6 | 2.38 | 0.0003277 |
| 7 | 2.88 | 0.0003218 |
| 8 | 3.37 | 0.0002785 |
| 9 | 3.86 | 0.0002693 |
| 10 | 4.38 | 0.000232 |
| 11 | 4.91 | 0.0002345 |
| 12 | 5.37 | 0.0002155 |
| 13 | 5.88 | 0.0002005 |
| 14 | 6.37 | 0.0001849 |
| 15 | 6.87 | 0.0001714 |
| 16 | 7.36 | 0.0001561 |
| 17 | 7.88 | 0.0001488 |

# APPENDIX B

# ACTINOMETRY DATA

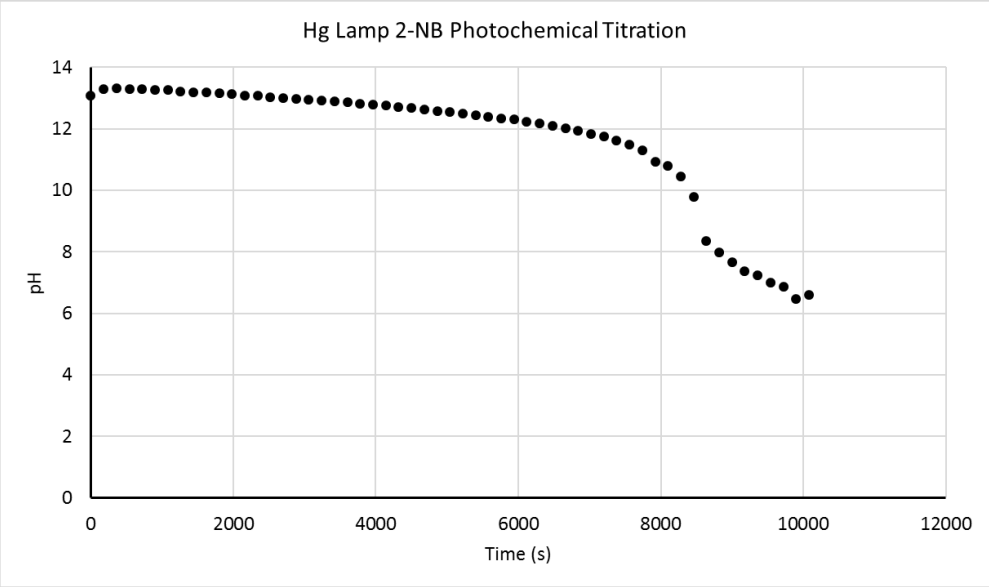


Figure 14 Hg Lamp 2-Nitrobenzalehyde Photochemical Titration

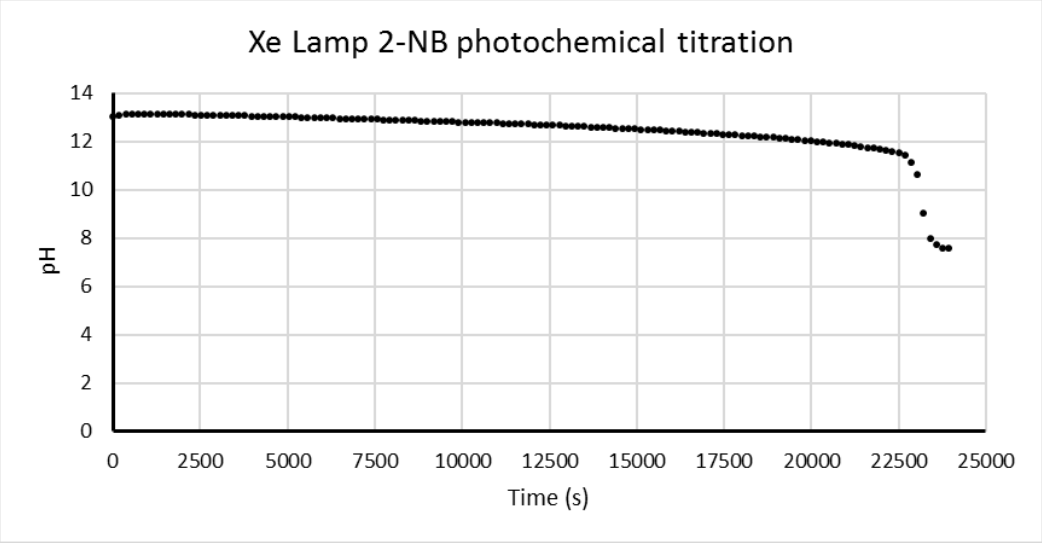


Figure 15 Xe Lamp 2-Nitrobenzalehyde Photochemical Titration

To determine endpoints for the titrations, the method used in Gran 1952 was used. 6 points near the pH inflection point were plotted with $(10^{pH})$*(time) vs time. The x intercept of a linear regression of the points is the time to the endpoint of the titration (Gran 1952). The time to the titration endpoint of pH 8.5 were 8300 s for the Hg lamp and 23000 s for the Xe lamp.

# APPENDIX C

# QUANTUM YIELD CALCULATIONS

Quantum yield is defined as number of Fe(II) atoms oxidized divided by number of absorbed photons.

$\Phi$ = Number of Fe atoms oxidized / $N_{photons}$

We calculated an average quantum yield, for all wavelengths < 345 nm, considering the Fe species $Fe(OH)^+$ and $Fe(H_2O)_6^{2+}$ to be photochemically active.

$\Phi$ was determined by the rate of Fe oxidized during the time the solution was exposed to the full lamp spectrum multiplied by the length of time exposed to the full lamp spectrum. This was used rather than simply finding the difference in [Fe] between the first and last data points as it takes all measurements into account and minimizes the influence of error in one point. The rate of Fe(II) oxidation is from a least-squares linear regression of the data for the time points over the region.

$N_{photons}$ was calculated using incident photons and absorbances for the Fe species considered ($Fe(OH)^+$ and $Fe(H_2O)_6^{2+}$). The path length in the reactor was 6 cm.

$$Nphotons = \int_{220\ nm}^{345\ nm} F_\lambda * (\varepsilon_{Fe(OH)^+}(\lambda)\ [Fe(OH)^+]\ L + \varepsilon_{Fe(H_2O)_6{}^{2+}}(\lambda)\ [Fe(H_2O)_6{}^{2+}])\ L\ d\lambda$$

$\Phi$ is the quantum yield

$\lambda$ is wavelength

$F_\lambda$ is the number of photons at wavelength $\lambda$

L is the path length

$\varepsilon_{Fe(OH)^+}(\lambda)$ is the molar absorptivity of $Fe(OH)^+$ at wavelength $\lambda$

$[Fe(OH)^{+}]$ is the concentration of $Fe(OH)^{+}$

$\varepsilon_{Fe(H2O)62+}(\lambda)$ is the molar absorptivity of $Fe(H_2O)_6^{2+}$ at wavelength $\lambda$

$[Fe(H_2O)_6^{2+}]$ is the concentration of $Fe(H_2O)_6^{2+}$

Photons < 345 nm were determined using the photon flux determined by actinometry and spectrometer measurements of the lamp spectrum (converted to photons $s^{-1}$ $nm^{-1}$) for the lamp's relative photon distribution at wavelengths below the 400 nm where the 2-nitrobenzaldehyde actinometer absorbs.

$N_\lambda$ = Percent of total photons < 400 nm at $\lambda$ measured by spectrometer * total photon flux < 400 nm

Quantum yield error was propagated from the standard error in the mol Fe oxidized (calculated from the linear regression) and allowing for a 10% error in photon flux measurements.